Deep Mining 2024 – P Andrieux & D Cumming-Potvin (eds)

doi:10.36487/ACG_repo/2465_17

Experiences of seismic monitoring at the Kittilä mine

Antti Pyy [a,*], Stephen Meyer [b], Véronique Falmagne [c]

[a] *Kittilä mine, Agnico Eagle Mines, Finland*

[b] *Institute of Mine Seismology, Canada*

[c] *Agnico Eagle Mines, Canada*

Abstract

The Kittilä gold mine in Northern Finland is owned and operated by Agnico Eagle Finland. The mining operation started in 2008 with open pits which were closed in 2012, when production moved underground. The new 1,040 m-deep hoisting shaft commenced operation in 2023. The mine consists of four separate orebodies, currently producing 2.0 Mt per annum, and requiring over 13 km of development on an annual basis. The principal mining method is longhole stoping with delayed backfill.

A microseismic monitoring system was installed during early development of the Rimpi orebody. Early development and mining of the Rimpi orebody between 700 to 900 m depth from surface indicated a potential for generating a dynamic rock mass response. The evolution of the rock mass response during the development and extraction of two upper (700 to 900 level) and one lower (1,025 to 900 level) pyramid(s) is presented, including the yielding sill pillar below 900 level and stress redistribution around the stoping areas.

An analysis of footwall structure activation and seismic response is presented with two examples. In both cases, stress change induced by stope extraction caused seismic events in the footwall at 50–200 m distance from the stoping.

Good location accuracy of seismic events (MW > −2.3) together with routine source mechanism calculation has enabled analysis of the seismically active structures in the footwall and improved ground support planning. Microseismic monitoring is an integral part of the Kittilä mine operational safety and seismic risk management.

Keywords: *microseismic monitoring, rock mass response, sill pillar*

1 Introduction

Kittilä mine is an underground gold mine owned and operated by Agnico Eagle Mines. The mine site is 150 km north of the Arctic Circle at 66° latitude. Operations started simultaneously with open pit production and underground development in 2008. Production moved underground in 2012 when the open pits were closed. The mine consists of four separate orebodies (Suuri, Roura, Sisar and Rimpi) currently producing 2.0 Mt per annum and requiring over 13 km of development on a yearly basis (Figure 1). Ore is transported to the surface via a 1,040 m-deep hoisting shaft and rockline that commenced operation 2023.

Mineralisation is located in the Lapland greenstone belt within the sub-vertical north–south Kiistala shear zone. Gold is more than 95% refractory, located in arsenopyrite and pyrite. Ore lenses show pinch and swell geometry causing variable grade distribution along strike and depth. The shear zone´s undulating joint surfaces have thin graphite schist coating. The longhole stoping method is transverse and longitudinal, with delayed cemented paste fill (CPF) for primary stopes and rockfill for secondary stopes. Cemented rockfill is currently used only when CPF is not available during mill shutdowns.

* Corresponding author. Email address: antti.pyy@agnicoeagle.com

Stope sublevel spacing varies between 25–40 m, stope footwall to hanging wall thickness ranges from 7–60 m and strike length is 15–30 m. Mine dewatering quantity is ~600 m^3/h in average.

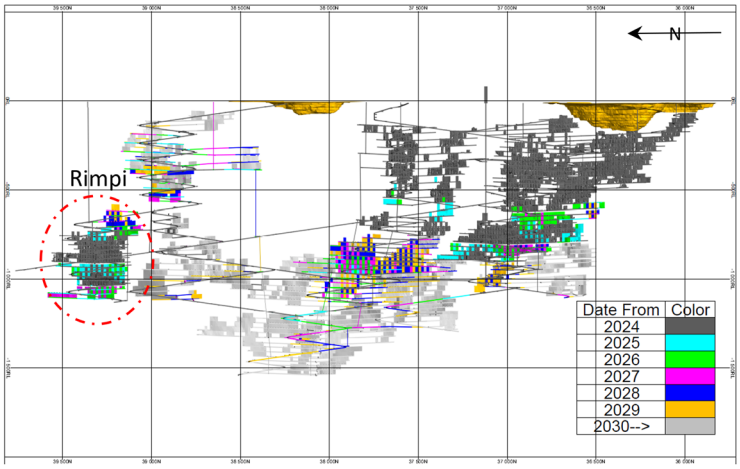

Figure 1 Longitudinal image of the life of mine plan. Mined-out stopes are in dark grey, with planned stoping according to colour scale, 500 × 500 m grid (Agnico Eagle Finland 2024)

2 Microseismic monitoring

An initial microseismic monitoring system was installed in Suuri in 2017 with the objective of evaluating what seismicity is recorded and what kind of data different sensors provide (Pyy et al. 2022). The first expansion of the system was installed in Rimpi between levels X925 and X850 before the stoping started in 2018. During development of the upper part at X775 level, MW = 1.6 rockburst took place. Study of the incident showed a fault-slip-type event on the thin footwall structure that triggered local strainbursts in the footwall haulage drift and crosscut. The seismic system was expanded at Rimpi after the incident. Seismic data is routinely processed by the Institute of Mine Seismology. The following chapters present the evolution of seismicity each year.

2.1 2020–2021

The Rimpi X900 mining panel was divided into two pyramids for the production requirements. The northern part of the panel has shown a higher seismic response from the beginning. The suspected reason for this is brittle behaviour of the footwall host rock: silicified mafic pillow lava with UCS > 300 MPa. Converging mining fronts induced higher seismic activity in between the pyramids (Figure 2).

Secondary crosscuts are normally developed after the adjacent primary stopes have been mined out and backfilled. Seismicity is not usually encountered with secondary crosscut development. However, in the the merger area of the panels, post development blast seismicity (MW > 0) was recorded. Before more sensors were added to lower levels, event locations below the bottom of the panel (X900 level) were suspected to have reduced location accuracy due to the poor sensor geometry. The initial system installed in 2019 consisted of six 14 Hz geophones (two triaxial and four uniaxial sensors) located in footwall decline. Sensors were aligned north–south, with available sensor locations being restricted to the main footwall ramp. This north–south configuration of the array resulted in greater east–west location uncertainty, as well as greater uncertainty for events near the top or bottom of the array. The network has since been updated in stages to the current seven triaxial and 13 uniaxial 14 Hz geophones, with a 4.5 Hz geophone installed 2 km south of Rimpi in the Suuri orebody.

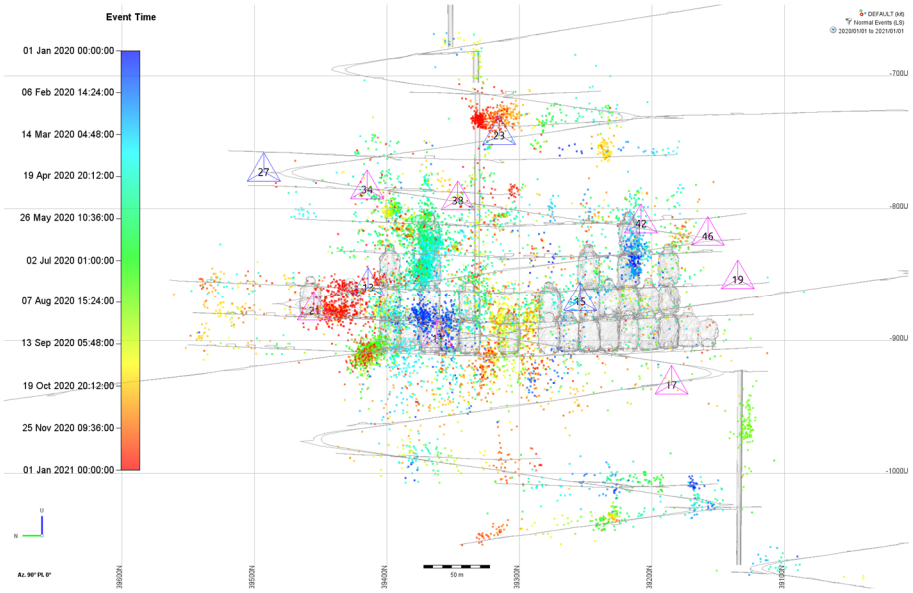

Figure 2 Rimpi seismicity from January 2020 to January 2021 in a longitudinal image looking east. Spheres are coloured by the time of the event. Mined-out stopes are presented in grey surface models with grid spacing of 100 m

2.2 2021–2022

With the progression of the two X900 mining fronts, the difference of the footwall and mineralised zone seismicity became clearer (Figure 3). Footwall seismicity is related to movement on thin brittle structures with fault-slip-type events while seismicity around the stoping area can be attributed to the yielding rock mass with a crush-type source mechanism. (Pyy et al. 2022) Two sensors were installed into a competent hanging wall rock utilising 45 m-long diamond drill holes drilled from the X700 level crosscut, with sensor 51 visible in Figure 3b. Adding sensors to the hanging wall has further improved network coverage for the source mechanism calculation.

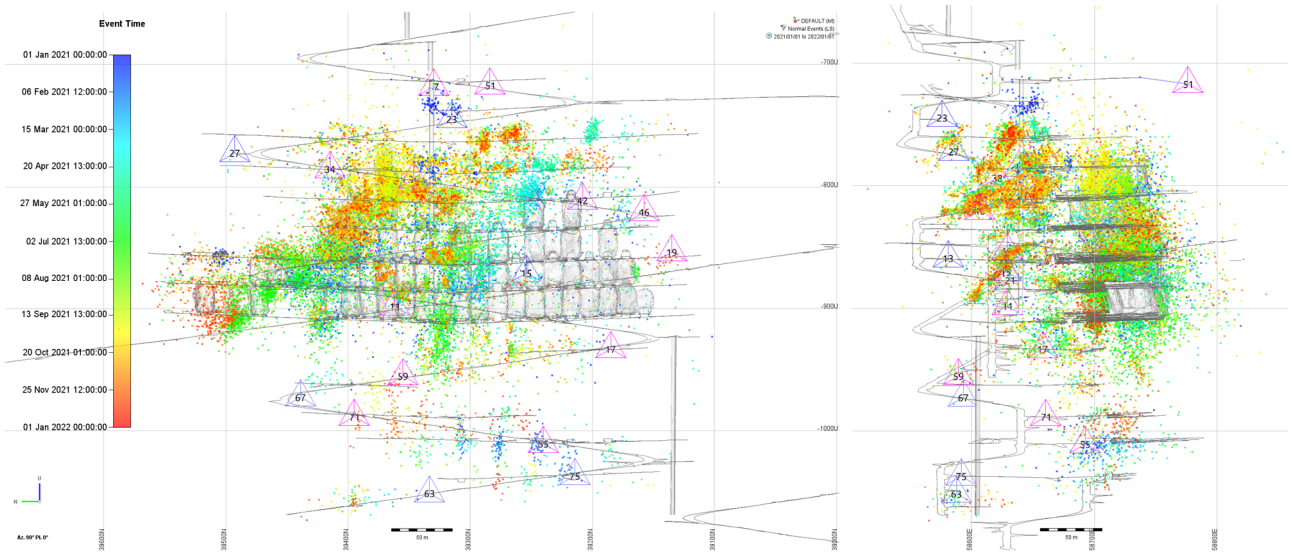

(a) (b)

Figure 3 Rimpi seismicity between January 2021 and January 2022: (a) Longitudinal view towards the east; (b) Section view along the strike towards north

2.3 2022–2023

Stoping from the X1025 panel started during 2022. Seismic response around the first stopes was small in comparison to the response of the upper panel. Most of the events in the X900-X1025 panel shown in Figure 4 are around footwall and crosscut development.

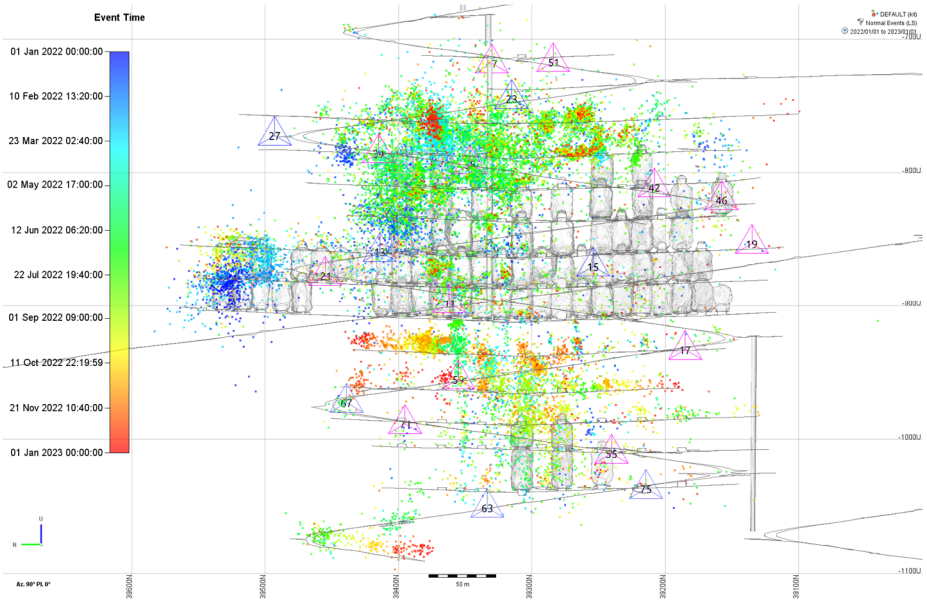

Figure 4 Rimpi seismicity from January 2022 to January 2023 longitudinal view

The stoping method at Rimpi is mostly transverse primary–secondary stoping. In the thinner fringe areas, a centre-out sequence is followed in order to push the stresses outwards to the abutment. The pinch and swell nature of the mineralisation is evident in the northern part of X900 level stopes with a gap in stoping. The mineralised shear zone continues through the area but the grade is below cut-off.

Development of the first crosscuts under the sill started in 2022. Figure 5 shows photo of the transverse access face at X925 level with sub-horizontal fracturing in the back. Horizontal jointing is not typically encountered and is believed to be related to stress-induced fracturing after mining of the upper stopes. Induced seismicity during the development was mostly MW < −1 and did not release enough energy to induce fracturing, which endorses the earlier. Figure 6 shows section view of the seismic data from the same area. During mining of the stopes above X900 level the seismicity extended below the X925 level.

Figure 5 Crosscut face at X925 level, 25 m below the sill and looking east towards the hanging wall. Visible horizontal stress-induced fracturing is in the back. Heading width is 5.8 m and height is 5.0 m. Sub-vertical graphite surfaces are visible on the face, typical to the mineralisation

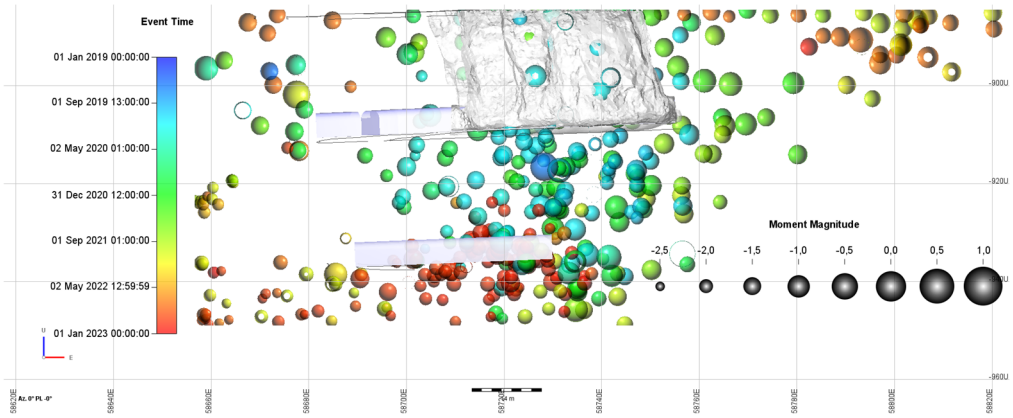

Figure 6 Temporal evolution of seismicity around the X925 level crosscut development with a 23 m-thick spatial filter towards the view of the image. Red coloured events are during the 2022 development

With the development progressing in the lower pyramid, planar clusters of small events (MW < −1) were recorded at X925 level. Events around the development in the northern part show mostly crush-type sources. Events 20 m west of the haulage drift are mostly slip-type events related to structures (Figure 7). Source mechanism calculations to events of MW > −2.3 enable verification of earlier structural interpretation of the area. Monitoring the behaviour of a distinct structure in response to stoping highlights areas requiring increased ground support where activated structures intersect the footwall development.

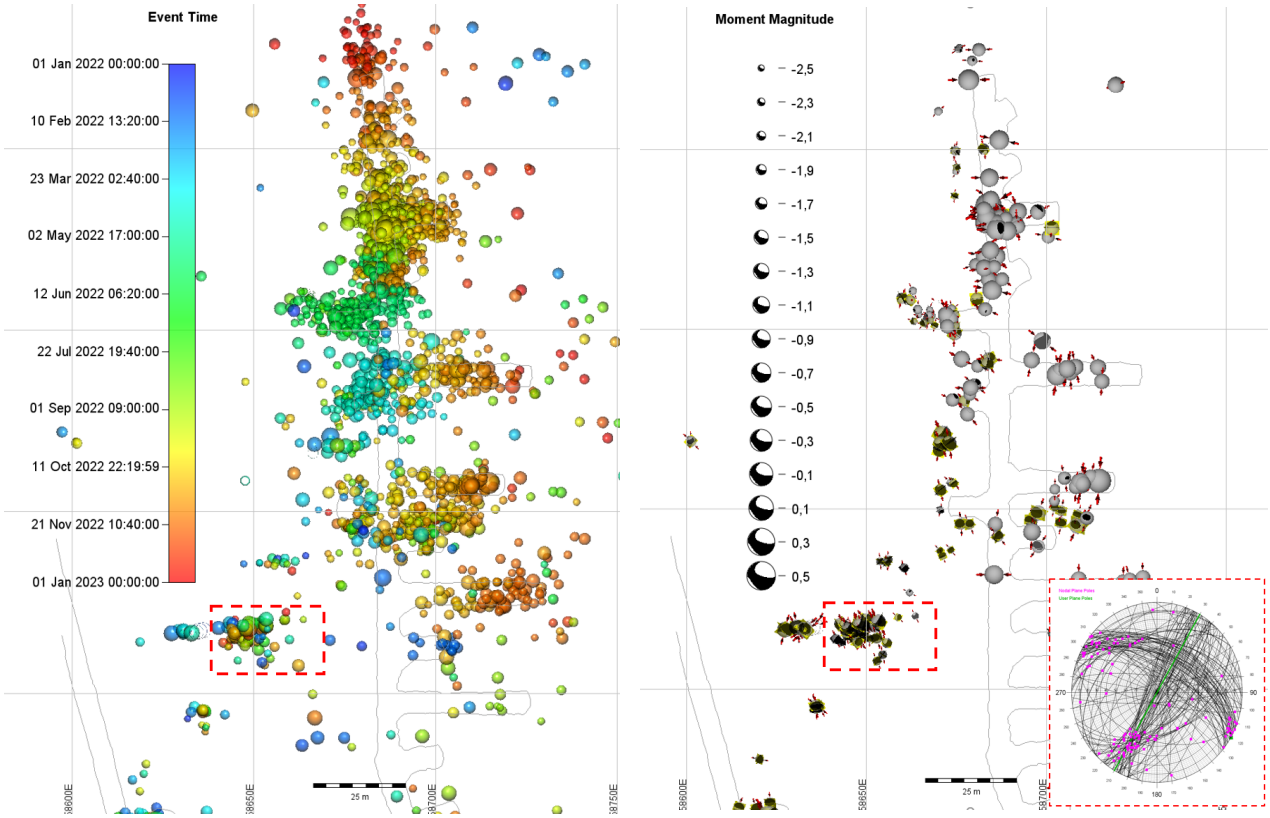

(a) (b)

Figure 7 X925 level: (a) Spatial-temporal evolution; (b) Calculated source mechanisms of the same event set. Pressure axis at red arrows. Stereonet of the highlighted events´ nodal planes are presented in the lower corner

2.4 2023–2024

During late 2023, mining progressed towards the X925-X900 sill pillar area. (Figure 8) Mining of the upper pyramids progressed upwards while secondary stopes were extracted in the middle of the area. There is usually very little seismicity recorded next to the secondary stope blast, indicating yielded rock mass, with the response being mostly located in the footwall structures. In late 2023 a secondary stope (X850L330) caved, with a 25 m-high block that failed downwards after the slot blast (marked in Figure 8). Both the footwall and hanging wall contacts have low-friction graphite schist on the joint surfaces. Recovery of the stope is still ongoing where the upper secondary stope was mined and backfilled with CPF prior to the salvage operation. The plan is to redevelop the overcut through the paste. The operation has an earlier experience of an 80 m-high block movement in a secondary stope in the upper Roura R350 mining block (Pyy & Falmagne 2019).

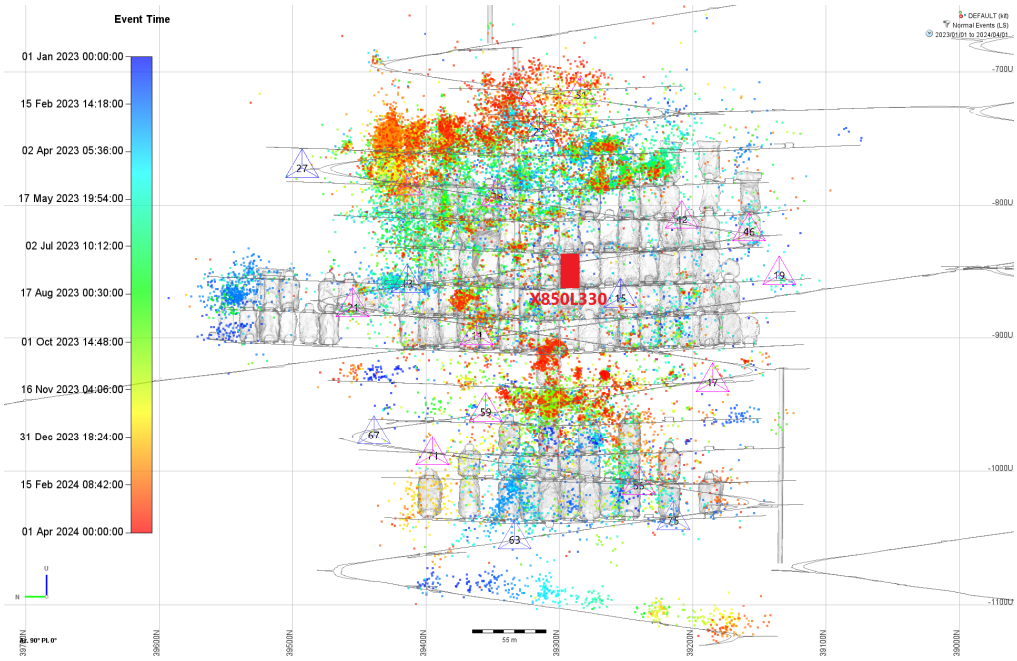

Figure 8 Rimpi seismicity between January 2023 and April 2024, longitudinal view

Observed seismicity after the extraction of the sill pillar stope X925L331 (Figure 9) was located on the footwall structures. This, combined with observed stress fracturing at the X925 development, suggests the sill had already yielded and that observed seismicity is due to change in the stress orientation.

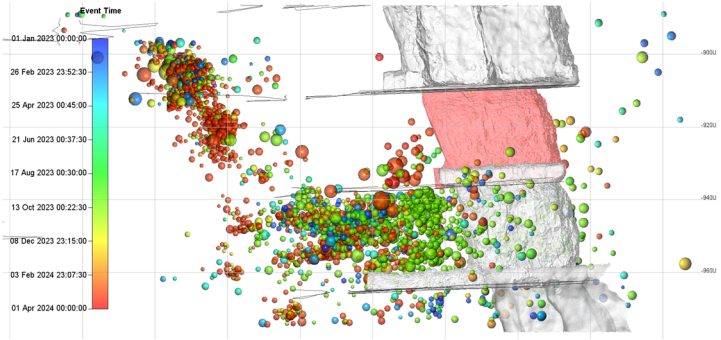

Figure 9 Section view of the X925-X900 sill pillar stope X925L331 (in red) blasted in March 2024. 20 m-thick spatial filter towards the view of the image (north). Colour scale of the events is the same as in Figure 8

The sill pillarblast was undertaken relatively close to the time this text was being written, so more time is needed for follow-up. However, an increased number of higher magnitude (MW > 0) events have been recorded in Rimpi since the blast (Figure 10).

The Rimpi footwall slip events have small isotropic components. Experience has shown that a relatively large (MW1.3, E = 10^6 J) slip event can be located ~15 m distance to development without visible damage to the excavation, with fibre-reinforced shotcrete (FRS), mesh surface support and yielding rockbolts.

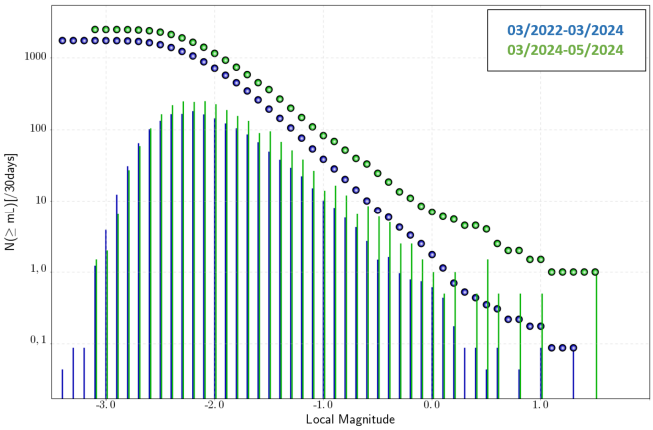

Figure 10 Magnitude distribution two years before and two months after the March 2024 sill pillar stope blast

2.5 Migration of seismicity on footwall structure

A few of the footwall structures had been identified during previous studies (Pyy et al. 2022). While seismicity continued to be observed on these structures, and newly identified ones with similar orientation were observed, an interesting observation was the spatial migration of seismicity on some of the structures over time. Figure 11 examines the seismicity on one of the more active structures. When first identified in 2021, seismicity was more to the north, around Y = 39270 – 39330, with P-axes trending sub-horizontal almost east–west (azimuth 100/280). Over the course of 2022 and 2023, seismicity migrated southward (more red in Figure 11a and more blue in Figure 11c) and the P-axes rotated more towards northwest–southeast (more red in Figure 11b). This trend is likely due to changes in the induced stress field around the stopes, influenced by the progressive yielding zone.

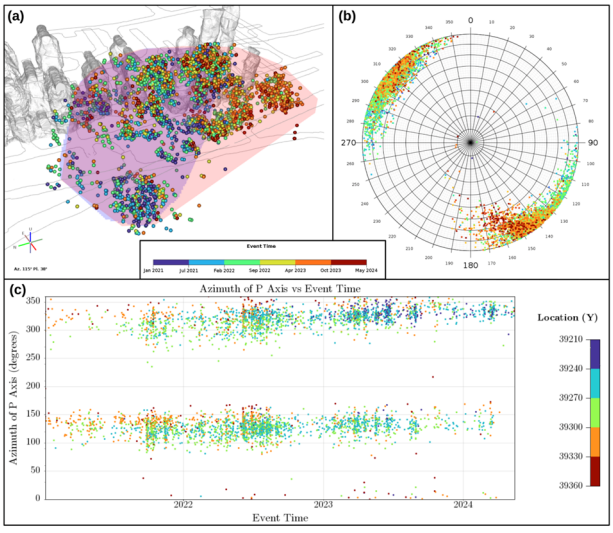

Figure 11 Slip-type events located within 10 m of the inferred structure and with a nodal plane within 25˚ of the structure: (a) Oblique view showing the spatial migration of seismicity over time. The darker shaded area represents the region originally identified in 2021 while the lighter red region shows where it expanded to over time; (b) Pressure-axes of source mechanisms of the events, coloured according to event time, showing a clockwise rotation as time progressed; (c) Azimuth of the P-axes over time, coloured by northing coordinate, also showing a slight but clear and consistent rotation of the events over time, moving south

3 Case studies

3.1 X800 pillarburst

In June 2022, a MW1.0 pillarburst took place after a nearby primary stope blast. The event happened during the post-blast exclusion protocol and damage was limited due to proactively increased ground support. The event was, however, of a larger magnitude than previously recorded in the area. A complete record of the seismicity was available from the surrounding area for forensic analysis. Ground support loading was also observed in the area, with cracked FRS and bent rockbolt faceplates prior to the event. Figure 12a presents immediate seismicity after the stope blast. The MW1.0 event location matches the observed damage in the local pillar between the sump and exhaust air raise access. (Figure 12b). On a larger scale, the event is located in between the two mining pyramids.

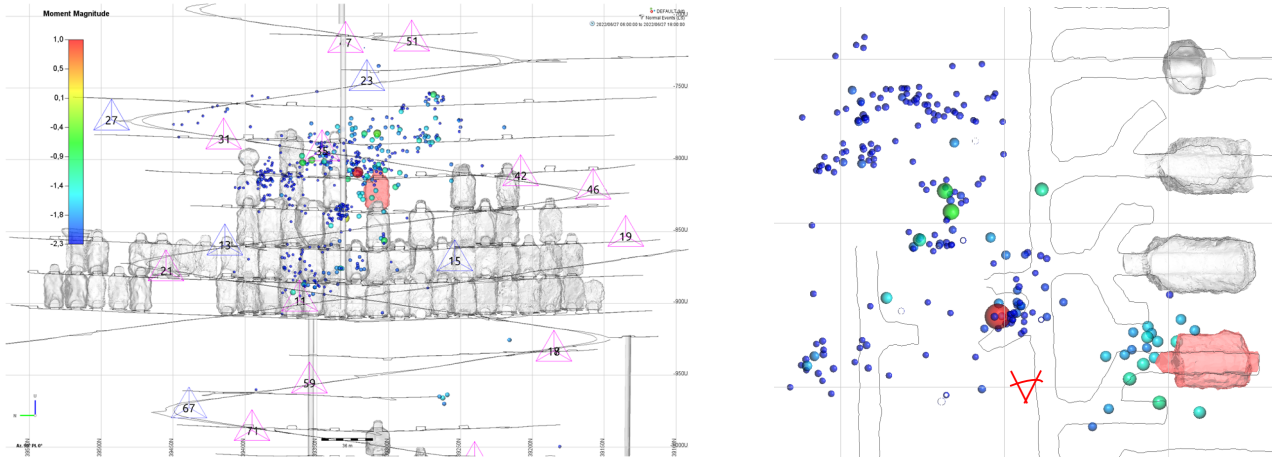

(a) (b)

Figure 12 Seismicity 12 hours after X800 footwall pillarburst: (a) Longitudinal image of the location; (b) Level layout of the event location. The blasted stope is in red with a red viewpoint marker for Figures 13 and 14a

Damage to the ground support located were in the non-upgraded (FRS and rebar) parts of the pillar walls (Figures 13 and 14). Upgraded parts of the support (welded mesh, mesh straps and yielding bolts) sustained the displacement and loading caused by the event.

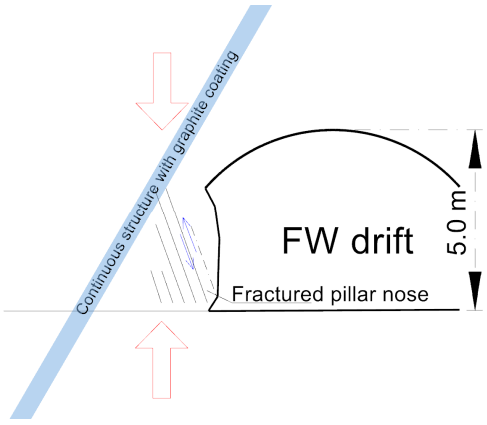

Figure 13 Schematic section view of the damaged pillar looking north. Red arrows indicate vertical loading of the pillar

(a) (b)

Figure 14 (a) Damaged toe of the local pillar, with visible loading on the mesh strap (Ø7.8 mm wire) and yielding bolt faceplate (2.4 m/8 ft Ø22 mm D-bolt) due to the pillar dilation. (b) Sheared horizontal 120 kN Mn Swellex inside the pillar shows the movement

Time history of the immediate surrounding area (Figure 15) shows several increases in the event activity rate. The energy index shows a decrease before the event, indicating progressive weakening of the pillar. The location accuracy of the events in this area is < 10 m with an updated adaptive apparent velocity model (Nordström et al. 2017). The filtered event set in Figure 15 contains 882 events, 437 of which have a source mechanism calculated.

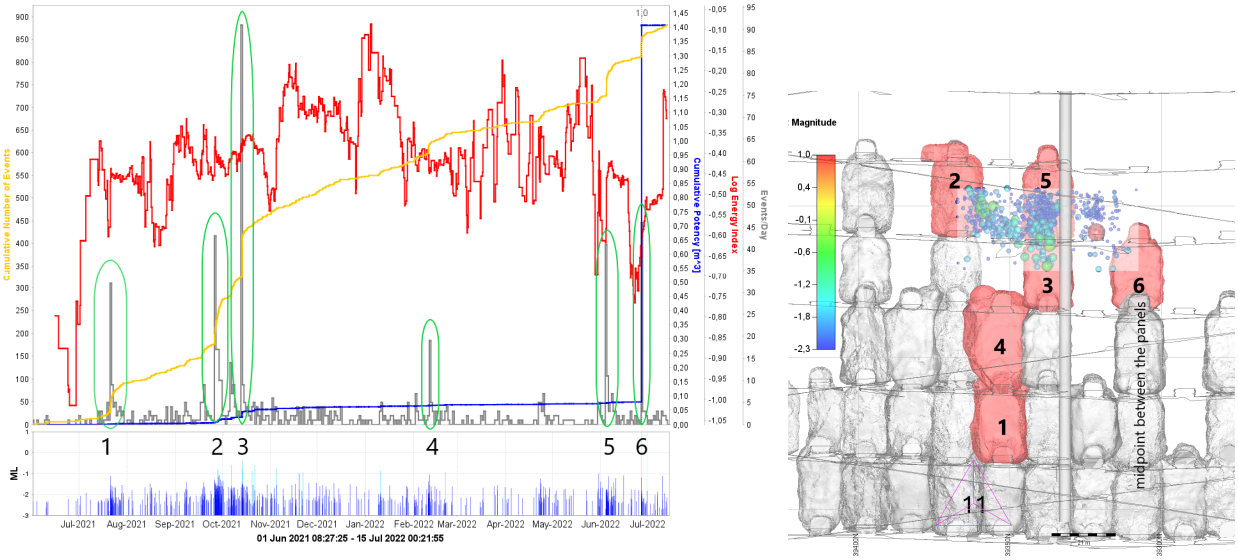

(a) (b)

Figure 15 (a) Time history of the area one year before the MW1.0 event. Increases in seismicity are marked with green ellipses, with numbering linked to mining of the stopes in (b); (b) Stopes that activated seismicity in the filtered area, with the dimension of filtering polygon l:58 m, w:34 m and h:27 m

Most of the events are small slip-type events (Figures 16a and 17) along a structure set on the west wall of the footwall drive. Most of the damage was caused by the MW1.0 burst event with higher potency in comparison to slip events with a total cumulative potency of ~0.05 m^3 (Figure 16b).

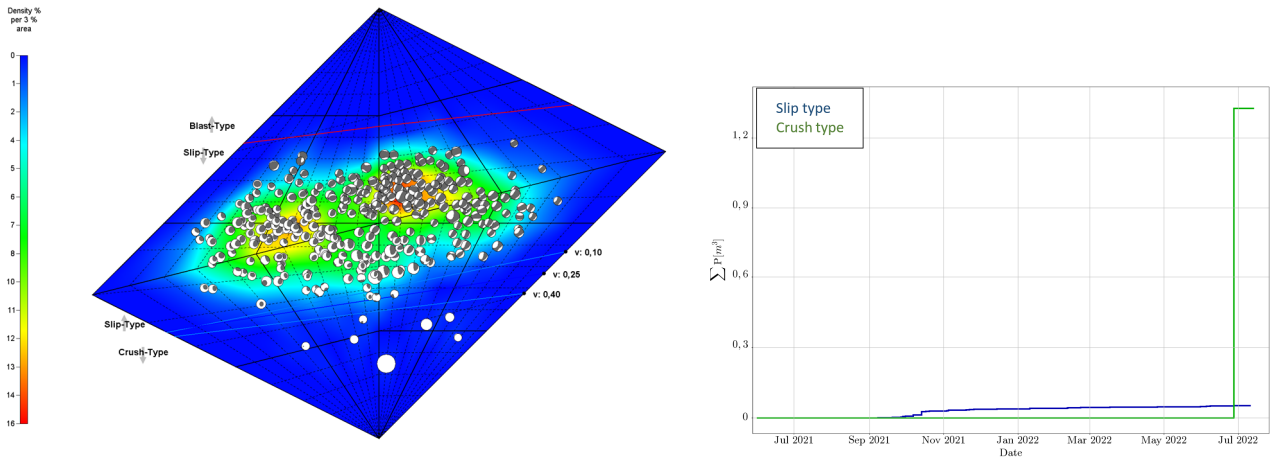

(a) (b)

Figure 16 (a) Hudson plot of the filtered event set, MW > −2.3; (b) Cumulative potency graph of the slip-type (blue) and crush-type (green) type events

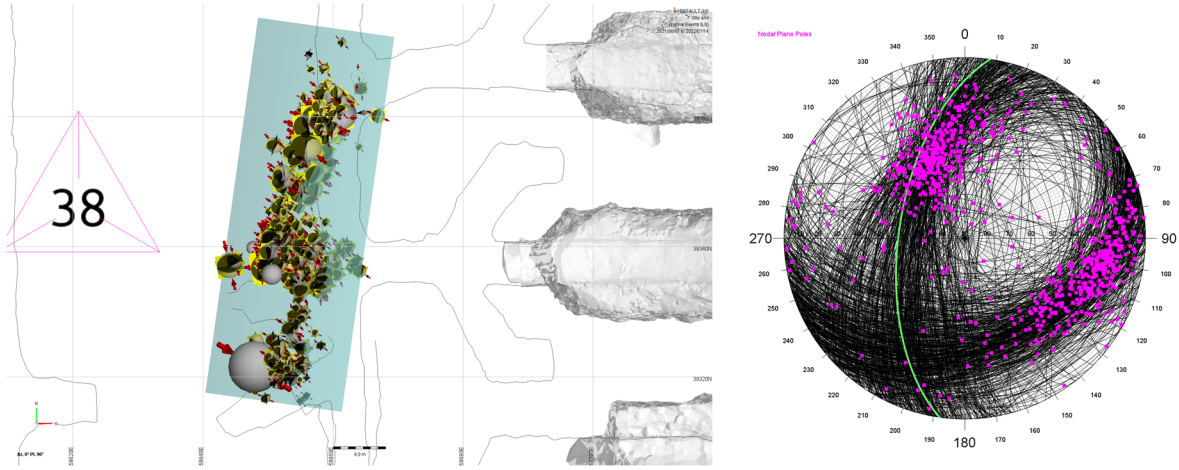

(a) (b)

Figure 17 (a) Level layout of the events with source mechanisms. Interpreted average plane of the structure (60˚/278˚, d/dd); (b) Stereonet plot of the event set nodal plane solutions with the inferred plane in green

In order to verify the seismic data observations, a numerical elastic model was built to test the effect of the mining sequence on the local pillar and structure (Figure 18a). Mid-pillar confinement (σ_3) decreases and loading (σ_1) increases during the mining steps/stoping advancement, indicating progressive weakening of the pillar. In-plane normal stress (σ_{ip}) decreases on the plane parallel to the weakness zone intersecting the pillar. Values from elastic modelling are indicative but concur with the actual monitoring results (Figure 18b).

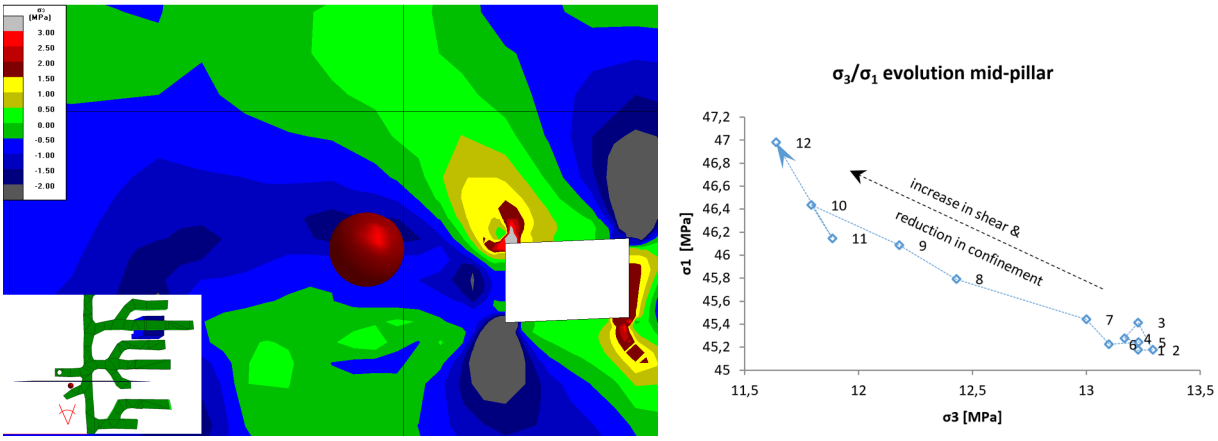

(a) (b)

Figure 18 (a) Section view of the modelled change in the confinement/minor principal stress σ_3 (from the year before to the time of the event) displayed on a vertical grid mid-pillar, MW1.0 event with red sphere, looking north, 25 m grid spacing. Similar viewpoint to Figure 13; (b) σ_3/σ_1 evolution over modelled mining steps

The complete record of the seismicity confirms the earlier hypothesis of seismically active planes intersecting footwall development. Small slip events caused progressive weakening of the local pillar and wider damage was caused by the MW1.0 crush-type event. Monitoring of the relatively small events provides good information for the forensic analysis and insight into the rock mass behaviour. Proactive rehabilitation of the drives with yielding ground support was proven as an effective measure to control the dilatation of the pillar. Mesh and dynamic rockbolts are currently being installed during the development cycle in Rimpi's deeper levels.

3.2 X700 fault slip event

In March 2024, one hour after a nearby stope blast, a rockburst occurred on the X700 level (Figures 19 and 20). Three MW > 0 events were recorded in the area. MW1.5 waveform is complex, starting as a reverse faulting event. The MW1.0 event source mechanism is crush-type, indicating sub-vertical loading to the intersection area. Smaller slip-type events were located in the footwall area. Development design between the level access and the exhaust air raise left a very narrow pillar in between creating an area of high local extraction ratio. The area was supported with static ground support (FRS and resin grouted rebar) which proved inadequate for the dynamic loading. The intersection back (span ø10 m) was also supported with 6 m-long cement grouted straight cables with plates in a 2 × 2 m pattern as part of the standard ground support for intersections. The cabled back remained stable.

The cluster of larger events was located 25 m above the Rimpi stoping at X700 level. Increased activity in the area started after the nearby longitudinal stope blast and small increases in the overall activity rate can be linked to stope blasts. A planar cluster was interpreted from the event locations and nodal plane solutions, indicating a fault activation along 130 m strike length with a reverse slip source mechanism (Figure 21a).

The model of the area highlights the narrow pillar in between the level access and the ventilation raise which matches the MW1.5 event location. The elastic model shows very small changes in excess shear stress between the mining steps, with the most critical factor being the fault plane location in relation to the development and ventilation raise (Figure 22).

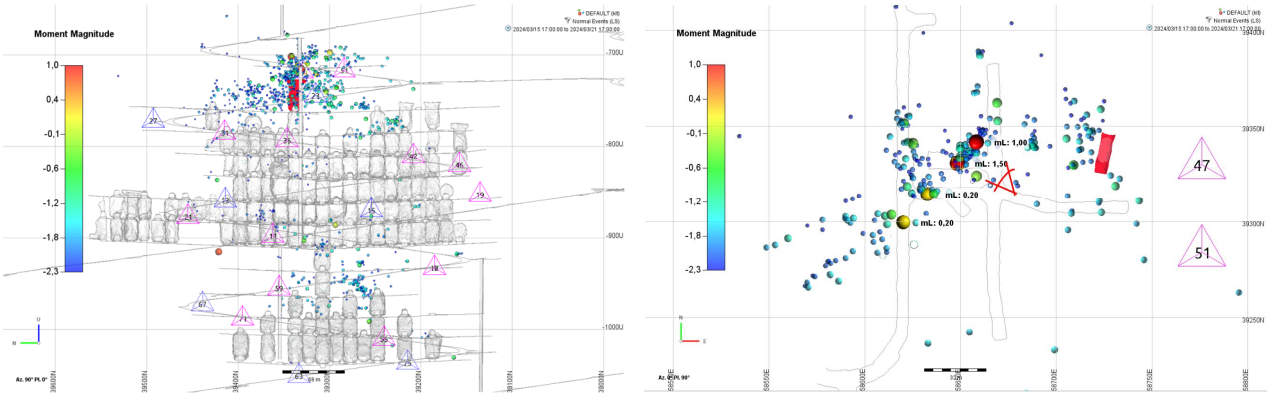

(a) (b)

Figure 19 X700 level events six days after the initial MW1.5: (a) Longitudinal view of the events in Rimpi, With the blasted stope that triggered the MW1.5 event in red; (b) Layout of the X700 level. Viewpoint of Figure 20 marked in red

Figure 20 Damages after the event in the intersection area of the footwall drive and exhaust air raise access, looking northwest

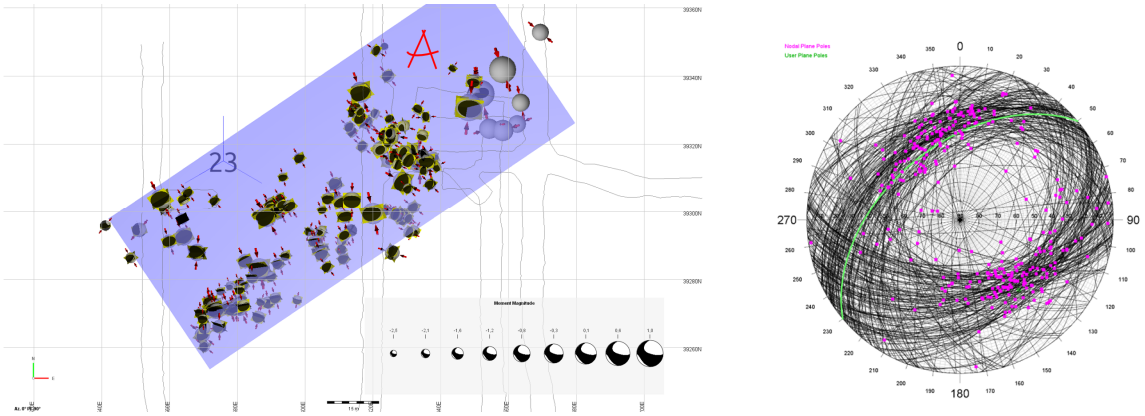

(a) (b)

Figure 21 (a) X700 events around the identified northwest-dipping planar cluster (in blue). Figure 22 viewpoint marked in red; (b) Stereonet of the calculated nodal planes with the inferred plane in green

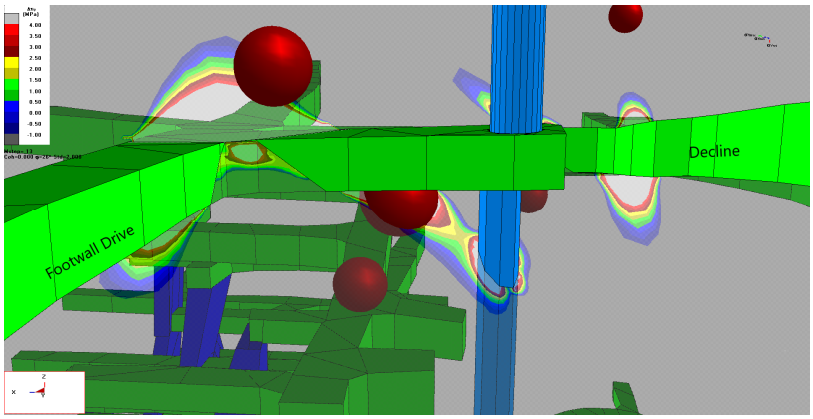

Figure 22 Modelled excess shear stress $\Delta\tau_{ip}$ on the plane (cohesion c = 0˚, friction angle φ = 28˚), MW > 0 events plotted with red spheres. View looking south

After the event, the ground support in the nearby decline was upgraded with mesh and yielding rockbolts. Two to three weeks after the event water seepage was observed through the damaged area intersected by the interpreted plane (Figure 23). Similar water seepage through increased porosity hydraulic conductivity of the structure was also noted after previous larger events in Rimpi.

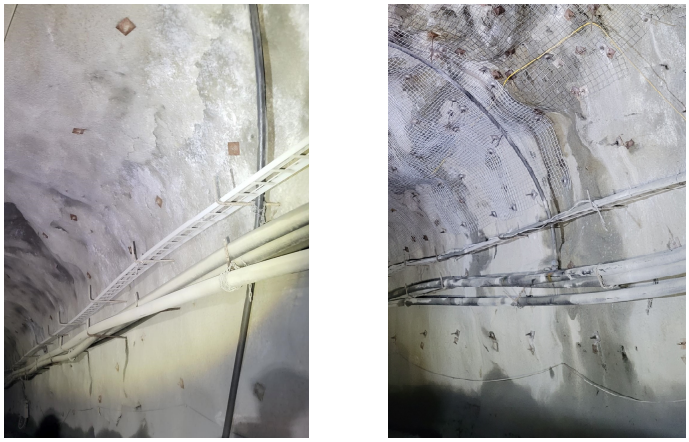

(a) (b)

Figure 23 Development intersected by the interpreted fault: (a) Immediately after the event the shoulder fibre-reinforced shotcrete shows bulging; (b) After additional ground support installation, water seepage from the structure intersecting the wall became visible

The analysis of the small events indicated previously unknown structures in the upper part of the Rimpi footwall intersecting the footwall drift and ramp. Back-analysis of area showed very small changes in seismicity prior to the damaging events. A high local extraction ratio next to the ventilation raise intersected by the fault was the key adverse element. Development of the parallel access to the ventilation raise from the footwall drive created a narrow span in between the ventilation and level access drives and the ventilation raise that was intersected by the indicated fault. The MW1.5 event was located in this gap. Static support was inadequate under dynamic conditions. The current Rimpi long-term development plan includes an updated ground support system to provide higher displacement and load capacity.

4 Conclusion

Seismic monitoring in Kittilä mine provides useful information of the rock mass response to mining. Calculation of the source mechanisms systematically down to MW > −2.3 events supplements the seismic record. Location of small slip-type events close to a development can identify structural interaction and help with the identification and tracking of previously unknown structures. The data presented here shows

excavation damage related to structure activation in a relatively shallow operation. The seismic data has provided better understanding of these events and improved ground control planning.

The presented case study of the local pillarburst at X800 level shows progressive rock mass weakening due to the small slip-type seismic events on structure intersecting the pillar. The larger crush-type event happened after the indicated increase in vertical loading and decrease in confinement. Damage was mostly contained by the upgraded ground support.

The rockburst on the X700 level was due more to sudden activation of the structure, and no clear precursory signs for an event of this magnitude were observed. Small slip-type events indicate structure continuity more than 130 m into the footwall.

Both cases are located close to the same ventilation raise and large-span intersections. This will be considered more carefully in future mine design and planning.

Microseismic monitoring is an important part of Kittilä mine ground control. Monitoring system will be expanded to new areas as the mine expands.

Acknowledgement

The authors would like to thank Agnico Eagle Kittilä mine management for permission to publish this paper and supporting the work conducted. Keeping the system operational is teamwork, and the authors thank the Kittilä mine and Institute of Mine Seismology personnel involved.

References

Agnico Eagle Finland 2024, *Life of Mine Planning*, internal document.

Nordström, E, Dineva, S, & Nordlund, E 2017, 'Source parameters of seismic events potentially associated with damage in block 33/34 of the Kiirunavaara mine (Sweden)', *Acta Geophysica*, vol. 65, no. 6, pp. 1229–1242, https://doi.org/10.1007/s11600-017-0066-1

Pyy, A & Falmagne, V 2019, 'Mining between graphite schist and variable quality backfill', *53rd Rock Mechanics/Geomechanics Symposium*, American Rock Mechanics Association, Alexandria.

Pyy, A, Meyer, S & Falmagne, V 2022, 'Early experiences of microseismic monitoring in Kittilä mine', *Proceedings of the 10th International Symposium on Rockbursts and Seismicity in Mines*, Society for Mining, Metallurgy & Exploration, Englewood.